9th International Conference on Numerical Ship Hydrodynamics
Ann Arbor, Michigan, August 5-8, 2007

Two Phase Level-Set/Immersed-Boundary Cartesian Grid Method for Ship Hydrodynamics

Jianming Yang, Nobuaki Sakamoto, Zhaoyuan Wang,
Pablo Carrica, and Frederick Stern
(IIHR-Hydroscience & Engineering, University of Iowa,
Iowa City, IA 52242, USA)

ABSTRACT

Recent progress at IIHR on the development of CFDShip-Iowa version 6 is presented. Current focus is on a sharp interface Cartesian grid method for the large-eddy simulation (LES) of turbulent two-phase incompressible flows. In this method, the level set formulation for two-phase incompressible flows is adopted. The density and pressure jump conditions across the interface (the latter due to surface tension and gravity) are treated in a sharp interface manner using the ghost fluid method. Complicated geometries immersed in the computational domain are handled with a sharp interface immersed boundary method. For LES, the Lagrangian dynamic Smagorinsky subgrid-scale model is used. Several approaches for capturing high Reynolds number boundary layers in a Cartesian grid layout are discussed. Simulations of several ship geometries, including the Wigley hull, DTMB model 5365 (Athena R/V), and surface combatant DTMB model 5415, have been carried out on relatively coarse Cartesian grids. Wave field patterns are successfully compared with experimental data and other computational results. To demonstrate the potential of coupled curvilinear/Cartesian grid methods, a case has been set up for model 5415 which utilizes the outer boundary layer velocity solution from a body-fitted RANS solver as boundary conditions for the immersed boundary method; very promising results have been obtained. The proposed developments needed to simulate high-Reynolds number boundary layers are briefly discussed.

INTRODUCTION

Milestone advances have been recently accomplished in CFD for ship hydrodynamics due to enabling technologies of surface capturing methods for free surface modeling of complex interfacial topologies and breaking waves, DES turbulence modeling of unsteady separated flows, and dynamic overset grids for complex geometries and motions/maneuvering. Successful verification and validation has been documented for a wide spectrum of applications ranging from resistance and propulsion to seakeeping to maneuvering with increased resolution of length and time scales, as evidenced by the papers at the 26th Symposium on Naval Hydrodynamics, including of interest herein CFDShip-Iowa version 4.0 (Carrica et al., 2006). As a result, realization of simulation based design for ship hydrodynamics seems assured. However, as high performance computers achieve petascale computing systems such that multi-scale and multi–physics problems with billions of grid points and degrees of freedom can be considered, increased accuracy, speed, and scalability of computations become pacesetting issues.

Cartesian grid approaches are good candidates for increased accuracy, speed, and scalability; however, they require special treatment to handle two-phase interfaces, complex geometries, and moving boundaries. For this purpose immersed boundary and cut cell methods have been developed. The former, originated by Peskin (1972), has been applied to solid/fluid interactions and then two-phase flow problems by many authors. The basic idea of immersed boundary methods is to model the effects of solid/elastic boundaries and fluid/fluid interfaces on the fluid flow by a set of body forces distributed over the nearby flow field of the immersed boundaries/ interfaces. In this force distribution process, the immersed boundaries/interfaces are smeared over several grid cells. In the past few years, several sharp interface methods using forcing or correction terms have been developed for solid-fluid and fluid-fluid interface problems. More details are referred to Yang and Balaras (2006), which presented a direct forcing immersed boundary method for moving boundary

problems, and the references therein. On the other hand, in the cut cell methods, the irregular cells produced by solid boundaries cutting through grid lines are treated in the same way as in an unstructured grid. In some versions of this type of methods the difficulties brought in by small cells were treated using cell merging technique, in which, essentially, a body fitted grid is generated at each time step for moving boundary problems. Although the cut-cell methods are sharp interface methods, they are very difficult to apply to three dimensional problems due to the large number of special treatments required by the numerous different interface cells generated during the cutting and merging process. The Cartesian grid methods discussed above have mostly been demonstrated for inviscid or low and moderate Reynolds number flows, mainly biological and physiological flows.

Applications of Cartesian grid methods in ship hydrodynamics have been advanced noticeably in recent years. Dommermuth et al. (2006) presented a Cartesian grid approach with immersed-body and volume-of-fluid methods. Remarkable ship waves from the simulations have been reported. However, as an incompressible Euler code with slip-wall boundary conditions used on the ship hull surface, their approach cannot capture boundary layers and the associated turbulence and wakes. Sussman (2005) developed a parallel, adaptive Cartesian grid approach with a coupled level set/volume-of-fluid method for interface capturing and an embedded boundary method for the immersed geometries. Although the adaptive mesh refinement strategy can give some flexibility on the grid and save some computational cost, boundary layers still cannot be resolved in his results due to the large number of grid points required as explained below.

At high Reynolds numbers the application of Cartesian grid methods becomes prohibitive, even with the use of local grid refinement, if the effects of boundary layer have not been taken into account properly. Taking the turbulent flow over a sphere as an example, as the Reynolds number increases, more grid points are needed to resolve the boundary layer. For body-fitted grids, a refinement in the wall-normal direction is necessary. However, for Cartesian grid methods the grids have to be refined in all three directions to obtain reasonable resolution near the wall, as a consequence of the non-alignment of grid lines and wall surface. Therefore, the total number of grid points for Cartesian grid methods increases much faster than that of body-fitted grids as the Reynolds number increases. Although the computational cost per grid point in Cartesian grid methods is much lower than that of body-fitted grids, there is a threshold in Reynolds number beyond which body-fitted grids become competitive in computational cost comparing to Cartesian grids. This threshold is well below the Reynolds numbers present in model scale ship hydrodynamics. In this context, a body fitted grid solving the near-wall boundary layer and a highly efficient Cartesian solver for the rest of the domain appears as the ideal approach to solve model and full scale ship flows.

Currently, IIHR is working toward CFDShip-Iowa version 6, a Cartesian grid solver that can handle the high Reynolds number boundary layers in ship flows. As a first step, a sharp interface method for two-phase flows interacting with complex structures has been developed. This method is based on the work of Yang and Balaras (2006), in which a 3D finite difference solver was developed for direct numerical simulation (DNS) and LES of turbulent flows with complex geometries and moving boundaries. This solver has been thoroughly restructured to a production level and extensively expanded to include many new components that are crucial to ship hydrodynamics applications. A level set formulation of the two-phase incompressible flows has been used and the free surface is handled in a sharp interface manner. High-order schemes for level set equations and momentum equations have been implemented. Highly efficient and scalable iterative solvers from PETSc library are used to solver the Poisson equations. High performance computing components, such as parallel tridiagonal system solver, parallel I/O, etc., are included. All these new additions together with the original capabilities provide us a high-fidelity, cost-effective, and simple-to-use Cartesian grid solver, which will be used as the infrastructure of the next generation simulation-based design tool for ship hydrodynamics, CFDShip-Iowa version 6. The detailed computational methods and verification/validation of this solver have been carried out through a series of test cases and reported in Yang and Stern (2007a, 2007b). In this paper, for the first time, CFDShip-Iowa version 6 is applied to two-phase ship flows. Initially, our attention is focused mostly on wave patterns, since no boundary layer is modeled at this stage. Very encouraging wave results were obtained for several ship hulls, including Wigley hull, model 5365 (Athena R/V), and the surface combatant model 5415. To demonstrate that the effects of high Reynolds number boundary layers can be taken into account in a Cartesian grid framework, a case has been set up for model 5415, which utilizes the outer boundary layer velocity solution from a body-fitted RANS solver as the boundary conditions for the immersed surface. Very promising results have been obtained for this case.

COMPUTATIONAL METHODS

The current method is based on the work of Yang and Balaras (2006) and has been extensively expanded to fit the need of ship hydrodynamics applications. The original solver was developed for DNS and LES of turbulent flows with complex geometries and moving boundaries. It features a fractional-step method for pressure-velocity coupling, a standard second-order central-differences scheme on a staggered Cartesian/ cylindrical grid, a second-order Adams-Bashforth or third-order low-storage Runge-Kutta scheme for time advancement, a fast Poisson solver using FFTPACK (Swarztrauber, 1984) and FISHPACK (Swarztrauber and Sweet., 1975), and a Lagrangian dynamics subgrid-scale stress model (Meneveau et al., 1996) for LES. The parallelization is done through a domain decomposition technique with MPI for the inter-processor communication. A sharp interface immersed boundary method has been developed to handle complex immersed stationary/moving boundaries on Cartesian grids.

On the basis of this solver, CFDShip-Iowa version 6 has been recently developed. A level set based formulation for two-phase incompressible flows has been introduced and a sharp interface treatment (ghost fluid method) of the free surface has been adopted. Correspondingly, a four-step fractional-step method for pressure-velocity coupling and a semi-implicit time advancement scheme have been employed. The level set evolution and reinitialization equations are solved using high-order TVD Runge-Kutta and WENO schemes. An improved particle correction method has been proposed and implemented to ameliorate the mass conservation properties of level set solver. Several high-order upwind convection schemes like QUICK and WENO have been added to solve the momentum equations. Highly scalable iterative (multigrid) solvers from the PETSc library have been used to solve the pressure Poisson equation. A parallel tridiagonal system solver has been implemented. Other new high performance computing components include parallel I/O and domain decomposition in arbitrary grid directions. All new components will be discussed in detail here as we introduce our current mathematical model, numerical method, and high performance computing strategies.

Mathematical model

The level set formulation for the incompressible flow of two immiscible fluids separated by an interface given in Chang et al. (1996) is used here. In this approach, one set of equations for both fluids are solved with the density and viscosity jumps across the interface linked by a Heaviside function.

Navier-Stokes Equations

Incompressible viscous flows of two immiscible fluids, e.g., air and water, are governed by the Navier-Stokes equations:

$$\frac{\partial \mathbf{u}}{\partial t} + \mathbf{u}\cdot\nabla\mathbf{u} = \frac{1}{\rho}\nabla\cdot\left(-p\mathbf{I}+\mathbf{T}\right)+\mathbf{g}\,, \tag{1}$$

$$\nabla\cdot\mathbf{u} = 0\,, \tag{2}$$

where t is the time, $\mathbf{u}$ is the velocity vector, p is the pressure, $\boldsymbol{I}$ is the unit diagonal tensor, ρ is the density, $\mathbf{g}$ represents the gravity acceleration, and $\mathbf{T}$ is the viscous stress tensor defined as

$$\mathbf{T} = 2\mu\mathbf{S} = 2\mu\left[\frac{1}{2}\left(\nabla\mathbf{u}+\left(\nabla\mathbf{u}\right)^{T}\right)\right] = \mu\left(\nabla\mathbf{u}+\left(\nabla\mathbf{u}\right)^{T}\right), \tag{3}$$

with μ the dynamic viscosity and $\mathbf{S}$ the strain rate.

Since the fluid properties are discontinuous across the interface, which is a function of time and space, density and viscosity are also functions of time and space and only known with given interface position. Their definitions will be deferred after the introduction of interface representation using level set.

Interface Jump Conditions

The velocity across the interface Γ is continuous, as the fluids are viscous and no phase change is considered here:

$$\left[\mathbf{u}\right] = 0\,, \tag{4}$$

and the jump condition for stress is

$$\left[\mathbf{n}\cdot\left(-p\mathbf{I}+\mu\left(\nabla\mathbf{u}+\left(\nabla\mathbf{u}\right)^{T}\right)\right)\cdot\mathbf{n}\right] = \sigma\kappa\,, \tag{5}$$

where [ ] indicates the jump at the interface, i.e., $f_L^I - f_G^I$ for a variable f with superscript I denotes interface, $\mathbf{n}$ is the unit vector normal to the interface, σ is the coefficient of surface tension, and κ is the local curvature of the interface.

Interface Representation

Defining the interface Γ as the zero level set of a signed distance function, ϕ, or the level set function, the position of the interface can be tracked by solving the level set evolution equation

$$\frac{\partial \phi}{\partial t} + \mathbf{u}\cdot\nabla\phi = 0\,. \tag{6}$$

To keep ϕ as a signed distance function in the course of the evolution, we iterate the reinitialization equation for the level set function (Sussman et al., 1994):

$$\frac{\partial \phi}{\partial \tau} + S\left(\phi_o\right)\left(\left|\nabla\phi\right|-1\right) = 0\,, \tag{7}$$

where τ is the pseudo time and $S(\phi_0)$ is a numerically smeared-out sign function

$$S(\phi_o) = \frac{\phi_o}{\sqrt{\phi_o^2 + h^2}}, \tag{8}$$

with ϕ_o the initial values of ϕ and h a small distance, usually the grid cell size, to smear out the sign function.

Fluid Properties

With the level set function defined, the fluid properties, such as density and viscosity, are given by the following equations:

$$\begin{aligned} \rho &= \rho_G + (\rho_L - \rho_G) H(\phi), \\ \mu &= \mu_G + (\mu_L - \mu_G) H(\phi), \end{aligned} \tag{11}$$

where the subscripts G and L represent gas and liquid phase, respectively, and the Heaviside function is defined as

$$H(\phi) = \begin{cases} 1 & \text{if} \quad \phi \geq 0 \\ 0 & \text{if} \quad \phi < 0 \end{cases}. \tag{12}$$

In this paper, the viscosity is smoothed over a transition region across the interface as

$$\mu = \mu_G + (\mu_L - \mu_G) H_\varepsilon(\phi), \tag{13}$$

using the smoothed Heaviside function (Sussman et al., 1994)

$$H_\varepsilon(\phi) = \begin{cases} 1 & \text{if} \quad \phi > \varepsilon \\ \frac{1}{2}\left[1 + \frac{\phi}{\varepsilon} + \frac{1}{\pi}\sin\left(\frac{\pi\phi}{\varepsilon}\right)\right] & \text{if} \quad |\phi| \leq \varepsilon \\ 0 & \text{if} \quad \phi < -\varepsilon \end{cases}. \tag{14}$$

Notice that with a continuous viscosity and velocity field, the stress jump condition Eq. (5) reduces to

$$[p] = p_L^I - p_G^I = -\sigma\kappa. \tag{15}$$

Subgrid-Scale Model

In the LES approach, the Navier-Stokes equations are spatially filtered such that the large, energy carrying eddies are resolved and the small scale, dissipative eddies are modeled by a sub-grid scale stress model. After applying the filter operation to Eqs. (1) and (2), we have

$$\begin{aligned} \frac{\partial \bar{\mathbf{u}}}{\partial t} + \bar{\mathbf{u}} \cdot \nabla \bar{\mathbf{u}} &= -\frac{1}{\rho}\nabla \bar{p} - \nabla \cdot \bar{\tau} \\ &\quad + \frac{1}{\rho}\nabla \cdot \left[\mu\left(\nabla \bar{\mathbf{u}} + (\nabla \bar{\mathbf{u}})^T\right)\right] + \mathbf{g} \end{aligned}, \tag{16}$$

$$\nabla \cdot \bar{\mathbf{u}} = 0, \tag{17}$$

where $\bar{f}$ denotes the filter operation on a variable f, $\bar{\tau} = \overline{\mathbf{uu}} - \bar{\mathbf{u}}\bar{\mathbf{u}}$ is the subgrid-scale (SGS) stress tensor, whose deviatoric part is parametrized following the Smagorinsky procedure as:

$$\bar{\tau} - \frac{1}{3}\mathrm{trace}(\bar{\tau})\mathbf{I} = -2\nu_t \bar{\mathbf{S}}, \tag{18}$$

and the turbulent eddy viscosity is defined as

$$\nu_t = C\Delta^2 |\bar{\mathbf{S}}|, \quad \text{and} \quad |\bar{\mathbf{S}}| = \sqrt{2\bar{\mathbf{S}} \cdot \bar{\mathbf{S}}}. \tag{19}$$

The model parameter C in the eddy viscosity definition has to be determined to close the equations. In this paper the Lagrangian dynamic SGS model (Meneveau et al., 1996) is chosen as it can handle complex geometries without the requirement of homogeneous direction(s). Therefore, Eq. (16) can be rewritten in the following form

$$\begin{aligned} \frac{\partial \bar{\mathbf{u}}}{\partial t} + \bar{\mathbf{u}} \cdot \nabla \bar{\mathbf{u}} &= -\frac{1}{\rho}\nabla \bar{p} + \nabla \cdot \left[\nu_t\left(\nabla \bar{\mathbf{u}} + (\nabla \bar{\mathbf{u}})^T\right)\right] \\ &\quad + \frac{1}{\rho}\nabla \cdot \left[\mu\left(\nabla \bar{\mathbf{u}} + (\nabla \bar{\mathbf{u}})^T\right)\right] + \mathbf{g} \end{aligned}, \tag{20}$$

with the trace of subgrid-scale stress tensor $\frac{1}{3}\mathrm{trace}(\bar{\tau})$ incorporated into $\bar{p}$.

Numerical Method

Navier-Stokes Solver

The finite differences method is used to discretize the Navier-Stokes equations on a non-uniform staggered Cartesian grid, in which the velocity components u, v, and w are defined at centers of cell faces in the x, y, and z directions, respectively, and all other variables, i.e., p, ϕ, ρ, μ, and ν_t are defined at cell centers. A semi-implicit time-advancement scheme is adopted to integrate the momentum equations with the second-order Crank-Nicolson scheme for the diagonal viscous terms and the second-order Adams-Bashforth scheme for the convective terms and other viscous terms. A four-step fractional-step method (Choi and Moin, 1994) is employed for velocity-pressure coupling, in which a pressure Poisson equation is solved to enforce the continuity equation:

- Predictor:

$$\begin{aligned} \frac{\hat{u}_i - u_i^n}{\Delta t} &= \frac{1}{2}\left(3A_i^n - A_i^{n-1}\right) \\ &\quad + \frac{1}{2}\left(C_i^{n+1} + C_i^n\right) - \mathrm{Grad}_i\left(p^n\right) \end{aligned}, \tag{21}$$

- First Corrector:

$$\frac{u_i^* - \hat{u}_i}{\Delta t} = \mathrm{Grad}_i\left(p^n\right), \tag{22}$$

- Pressure Poisson Equation:

$$\frac{\partial}{\partial x_i}\mathrm{Grad}_i\left(p^{n+1}\right) = \frac{1}{\Delta t}\frac{\partial u_i^*}{\partial x_i}, \tag{23}$$

- Second Corrector:

$$\frac{u_i^{n+1} - u_i^*}{\Delta t} = -\mathrm{Grad}_i\left(p^{n+1}\right), \tag{24}$$

where superscript n denotes time step, subscript i = 1, 2, 3 represents i-coordinate, A and C denote terms treated by the Adams-Bashforth and Crank-Nicolson schemes, $\hat{u}_i$ and u_i^* are the first and second intermediate velocities, respectively. $\mathrm{Grad}_i(p)$ is a pressure gradient term defined at the center of the cell faces (collocated with velocity components) with the jump conditions incorporated in it.

In Eq. (21) the convective terms are discretized using a third-order QUICK scheme (Leonard, 1979) and higher-order WENO schemes (Jiang and Shu, 1996) are available. All other terms are discretized with the standard second-order central difference scheme. Eq. (21) is approximated with the approximate factorization method (Beam and Warming, 1976) and the resulting tridiagonal linear equations are solved with the parallel tridiagonal system solver (Mattor et al., 1995). The parallelization is done via a domain decomposition technique using the MPI library. The pressure Poisson equation is solved using a multigrid-preconditioned Krylov subspace solver from the PETSc library (Balay et al., 1997). In general, this is the most expensive part of the whole algorithm.

Level Set Solver

The level set and the reinitialization equations are solved using a third-order TVD Runge-Kutta scheme (Shu and Osher, 1988) for time advancement and the fifth-order HJ-WENO scheme (Jiang and Peng, 2000) for spatial discretization. The solution time of these equations does not pose a significant overhead as they are solved in a narrow band several grid-cells wide as detailed in Peng et al. (1999).

The level set method suffers from severe numerical dissipation which results in a significant mass or characteristic information loss in the under-resolved regions. A particle correction step, based on a hybrid particle level set scheme (Enright et al., 2000), is available for more accurate interface representation. In this hybrid method, massless particles are introduced and used to correct the level set function in the under-resolved areas. It has been shown that a remarkable improvement in mass conservation on small scale flows (bubble entrainment, water splash, jet pinch-off, etc.) and the interface properly captured.

Immersed Boundary Treatment

The embedded boundary formulation in Yang and Balaras (2006) is adopted here to treat the immersed boundaries/bodies in a non-uniform Cartesian grid. In this approach, the grid generation for complex geometries is trivial since the requirement that the grid points coincide with the boundary, which is imperative for body-fitted methods, is relaxed; while the solution near the immersed boundary is reconstructed using momentum forcing in a sharp-interface manner. The detailed procedure is described in Balaras (2004), Balaras and Yang (2005), and Yang and Balaras (2006) and summarized here.

The first step is to establish the grid-interface relation with a given immersed boundary description, such as parametrized curve/surface or a triangulation. In this step all Cartesian grid nodes are split into three categories: (1): fluid-points, which are points in the fluid phase; (2) forcing points, which are grid points in the fluid phase with one or more neighboring points in the solid phase; (3) solid-points, which are points in the solid phase. The Navier-Stokes solver described in the previous section is applied on all points of the Eulerian grid as if the fluid/solid interface was not present. The effect of the immersed boundary on the flow is introduced through the discrete forcing function, which is computed only at the forcing points by directly enforcing the boundary conditions. In general, the velocity at the forcing points can be computed by means of linear interpolation that involves the projection of the forcing point on the interface and two points in the fluid phase. For the semi-implicit time advancement scheme used here, a provisional step is applied with all terms by the Crank-Nicolson scheme treated using the forward Euler scheme. Then the forcing function can be evaluated straightforwardly as in Kim et al. (2001) and Balaras and Yang (2005). The above procedure has been extensively tested for a variety of laminar and turbulent flow problems involving stationary and moving immersed boundaries with results in excellent agreement with reference computations and experiments as demonstrated in Balaras and Yang (2005), and Yang and Balaras (2006).

High Performance Computing

One of the major objectives of the development of CFDShip-Iowa version 6 is to make use of the on-coming petascale computers and provide fast turnaround for simulation-based design in ship hydrodynamics. The simple topologic structure of Cartesian grids is extremely favorable for coarse-grain parallelization. A simple domain decomposition technique is used in CFDShip-Iowa version 6 where the Cartesian grid is divided into uniform pieces, each of which resides in one processor. Optimal load balance can be achieved except for a small amount of overhead due to interface and immersed boundary treatment, which may be unevenly distributed over processors.

The parallel tridiagonal system solver by Mattor et al. (1995) is used with the approximate factorization (Beam and Warming, 1976) of momentum equations. For the pressure Poisson equation, a multigrid-preconditioned Krylov subspace solver from PETSc (Balay et al., 1997) has been included in the code. Usually, the Poisson solver takes more than 90 percent of the CPU time in a single time step.

Adaptive mesh refinement (AMR) methods combined with higher-order discretization schemes has been proved to be more effective for the numerical simulation of fluid flows with complex flow patterns and large range of spatial scales. AMR refines and de-refines the grid dynamically and locally with complete control of grid resolution and more flexibility, which makes the overall computational cost greatly reduced. PARAMESH (MacNeice et al., 2000), a software package developed at the NASA Goddard Space Flight Center, is used to implement the adaptive mesh refinement into CFDShip-Iowa version 6 with a load-balancing technique for parallelization. The level set equations have been successfully solved with the AMR technique, and identical results are obtained as those on a full domain uniform grid with decreased computational time. Combination of the flow solvers with the PARAMESH package is in progress.

RESULTS

Grid Design

The simulations presented in this study are summarized in Table 1. Tests 1, 2 and 4 were computed using CFDShip-Iowa version 6. Test 3 was run with CFDShip-Iowa version4 (Carrica et al., 2006). Test 5 was computed with CFDShip-Iowa version 6, but using a solution from the curvilinear two-phase level set solver CFDShip-Iowa version 5 (Huang et al., 2007) as velocity boundary condition.

An example of the types of grids used is shown in Fig. 1. Details of the grids for each test are presented in Table 2. In Test 3, overset grids are used in which the Cartesian coarse grid originally used for Test 2 is adopted as the background grid and the boundary layer is resolved by a body-fitted grid. The connectivity between the boundary layer and background grids is computed in a pre-processing step using the interpolation code SUGGAR (Noack 2005). The boundary layer grid has a spacing normal to the hull of $1.5\times10^{-6}L$. The turbulence is included with a Shear Stress Transport (SST) k-ω turbulence model (Menter, 1994).

The domain sizes adopted for each test are shown in Table 3. All simulations with the exception of Test 5 take advantage of the symmetry of the problem about the vertical centerplane and are computed in a half domain; Test 5 uses LES and a full domain was chosen. The boundary conditions used in the study are shown in Fig. 1.

Wigley hull

The case of a Wigley hull in steady forward speed advancing in calm water at $Fr = 0.267$ in even keel condition is studied first.

Figure 2 shows a comparison of the wave pattern obtained with CFDShip-Iowa version 6 and the experimental data from D'Este and Contento (2003). The Cartesian grid solver does a remarkable job predicting the wave pattern characteristics, including wavelength and amplitude. CFD results slightly under-predict the amplitude of the second trough. The Cartesian grid solution is better than the potential flow solution presented by D'Este and Contento (2003, not shown). This level of quality on the free surface solution can be achieved with inviscid flow solvers, since the boundary layer has little effect on the wave pattern with the exception of the wake region. Notice that our solution also fails at the transom, where the lack of a turbulence model results in an over-prediction of the wake velocity.

To show the effect of the grid spacing on the free surface pattern, a coarse grid solution is presented in Fig. 3, compared also with the solution from CFDShip-Iowa version 4, a single-phase level set solver. As expected, the fine grid gives a better resolution, though the results on the coarse grid are still good. Notice that the fine grid is only 7.4 million grid points, a modest number for the capabilities of Cartesian grids.

Considerably better results are obtained with the Cartesian grid solver as compared with the single-phase solver for the coarse grid. It must be noted that a single-phase computation would not have used the same grid design as the two-phase solver, but the comparison is still valid in that shows that for the same level of refinement at the free surface the higher-order Cartesian grid solver does a better job resolving the wave pattern. Possible reasons for the better resolution of the wave pattern on CFDShip-Iowa version 6 than in version 4 include (1) time averaging for RANS simulation results in more dissipation in free surface wave, and (2) the spatial discretization is less diffusive in version 6 (5^{th}-order WENO vs. 2^{nd}-order upwind). Notice that the solution at the wake is better in version 4 than in version 6. A clear over-prediction of the wake velocity caused by the lack of a boundary layer in the Cartesian Solver results in a smaller stern peak located further downstream.

Model 5365 (Athena R/V)

Athena R/V is a fairly streamlined vessel with a transom stern. This adds complexities on the flow, at low speed because it results in boundary layer separation, and at larger speeds because the stern wave breaks. At the selected speed ($Fr = 0.25$), the transom is wet and separation occurs (Wilson et al., 2006).

The wave pattern is compared against the experimental data by Fu et al. (2005) in Fig. 4. Details are shown for the bow and stern portions of the domain. Since the transom is highly unsteady, solutions were averaged for $3 < t < 5$. As in the case of the Wigley hull, the solution can adequately predict phase and amplitude of the wave system correctly. The very steep bow wave is captured, as is an indication of the shoulder wave at $x/L \approx 0.85$. In the transom the solution over-predicts the height of the rooster tail and the location of the peak. Wave cuts at several spanwise cross planes are also compared with the EFD data in Fig. 5. The agreement with the closest cross sections is excellent, and the solution deteriorates as we move farther out due to diffusion. This is a general trend in surface capturing free surface approaches, as can be seen in the results of several codes for this same case (Wilson et al., 2006). However, the results presented are at least as good as those obtained with different methods on finer grids. Figure 6 shows the vortical structures at the transom region using isosurfaces of the second invariant of the deformation tensor Q (Haller, 2005), Q=300 for air and Q=1,000 for water, colored by the axial vorticity. Rich small-scale structures are observed both in air and water, provided by a viscous solution. The large-scale separation vortices observed by Wilson et al. (2006) are not present, probably due to the absence of a turbulence model adequate to predict the boundary layer.

Model 5512

DTMB 5512 is a 3.048 *m* model of a surface combatant. As an additional geometrical complexity respect to the Athena R/V, it has a sonar dome on the bow. There is extensive data available for this ship at different model scales, including wave fields (Gui et al., 2001) and velocities at the nominal propeller plane $x/L = 0.935$ (Longo et al., 2007).

The computation was made starting at a distance from the hull ranging from $y^+ = 200$ to $y^+ = 900$, with most of the surface area with $y^+ \approx 400$, well within the boundary layer, see Fig. 7. At this point the Cartesian grid, immersed boundary solver uses the velocity field provided by the curvilinear solver, as it would do in a coupled approach. It must be noted that at this stage of development the Cartesian solver does not receive information of the turbulence from the curvilinear solver, and uses an independent LES approach.

The wave field compared against the experimental data (Gui et al., 2001) is shown in Fig. 8, that shows a plane section of the Cartesian grid used. The very coarse grid used in the far field results in a poor prediction of the wave field in that region, but satisfactory in the near field. Notice the good agreement between CFD and EFD in the wake area. In this computation the velocities used by the LES code are matching better the boundary layer, and thus the wake prediction is improved.

Figure 9 shows the vortical structures at the transom region using isosurfaces of the second invariant of the deformation tensor Q (Haller, 2005), Q=100 for air and Q=20 for water, colored by the axial velocity. Only large-scale structures are presented both in air and water as boundary layer turbulence is missing in the present solution-patching approach.

Velocity predictions at the nominal wake plane are shown in Fig. 10, compared with experimental data. The unsteady CFD results were averaged over $4.4 < t < 6.4$. Results of average and RMS fluctuations of velocity in all three directions are compared against ensemble-averaged experimental data of average velocity and normal Reynolds stresses. In general, the results obtained are promising, considering the overly simplified approach. As expected, the CFD computations under-predict the turbulence in the near-hull region and over predict it in the far field. The immediate consequence is that the sonar dome vortices remain stronger than in the experimental data, causing a more marked hook in the axial velocity distribution. Also the stronger vortices result in a larger vertical velocity at the symmetry plane.

CONCLUSIONS

The progress toward the development of CFDShip-Iowa version 6 was presented. At this stage of the development, a sharp interface Cartesian grid solver with combined level set and immersed boundary methods is operative. The modeling of the two-phase incompressible, viscous air/water flow with jump conditions at the interface was discussed. Numerical methods were presented and several ship hulls were used to validate the code. Very good wave fields have been obtained from the simulations. A case that utilizes the boundary layer velocity solution from a body-fitted grid has been demonstrated. The encouraging results show that the effects of high Reynolds number boundary layers can be incorporated into a Cartesian

grid solver through coupling with a curvilinear solver or some other means to resolve viscous boundary layers.

Currently, several approaches for capturing the effects of viscous boundary layers within the framework of a Cartesian grid solver are under consideration. In general, a series of strategies with different levels of complexity can be adopted. The simplest way is to use a wall function approach, in which the velocity distribution near the wall is no longer a linear profile; instead, a non-linear profile given by a specific wall function can be used. The reader is referred to Bhushan et al. (2007) in this conference for applications of wall functions in our body-fitted grid solver for model- and full-scale ship flows. Using wall functions in Cartesian grids would render a body-fitted grid unnecessary. However, this approach would require very fine grids even for model-scale problems. A more general way is to use advanced wall-layer models on a body-fitted grid, such as solving the turbulent boundary layer equations or even RANS equations with given pressure gradients, which can be extrapolated from the Cartesian grid solution. Also, a coupled curvilinear/Cartesian grid method is proposed to combine the advantages of both Cartesian and body-fitted grids. Curvilinear grids are used to resolve high Reynolds number boundary layers for complex geometries, which are combined with Cartesian grids for the bulk of the flow both of which enable increased accuracy, speed, and scalability. Our ultimate goal is to use orthogonal curvilinear grid solvers coupled with Cartesian grid solvers. An additional advantage of using orthogonal curvilinear grids (Nikitin, 2006) instead of non-orthogonal ones is that the discretization of the governing equations is very similar to that in Cartesian grids, and therefore the implementation is greatly simplified and the overall efficiency close to that of Cartesian grid methods.

For turbulence modeling, a series of options ranging from one- and two-equation turbulence models, algebraic Reynolds stress model, and detached eddy simulation (DES) have been built into CFDShip-Iowa version 4 (Carrica et al., 2006 and Xing et al., 2007). Hybrid RANS/LES approaches like DES or more advanced methods can produce much better results in some flows than RANS models, with computational costs much lower than that of wall-layer resolved LES. Besides the capabilities for turbulence modeling available in CFDShip-Iowa version 4, we also propose to solve a one- or two-equation RANS model in the wall-layer, and solve the filtered Navier-Stokes equations with Lagrangian dynamic SGS model (Meneveau et al., 1996) on the bulk Cartesian grid. This approach is expected to result in an improvement over the original DES method. Work on the proposed wall-layer treatments, hybrid RANS/LES approaches, and improved interface tracking schemes is in progress. All these components will be built into CFDShip-Iowa version 6, such that all current/planned CFDShip-Iowa version 4 capabilities for 6DOF, environmental effects, propulsor modeling, thermal and salinity transport, shape optimization, high performance computing, and user interface will easily transition to version 6.

ACKNOWLEDGMENTS

This research was sponsored by the Office of Naval Research under Grant N00014-01-1-0073 and N00014-06-1-0420, under the administration of Dr. Patrick Purtell.

REFERENCES

Balaras, E., "Modeling complex boundaries using an external force field on fixed Cartesian grids in large-eddy simulations," Computers & Fluids, Vol. 33, 2004, pp. 375-404.

Balaras, E. and Yang, J., "Non-boundary conforming methods for large-eddy simulations of biological flows," ASME J. Fluids Engineering, Vol. 127, 2005, pp. 851-857.

Balay, S., Gropp, W.D., McInnes, L.C. and Smith, B.F., "Efficient Management of Parallelism in Object Oriented Numerical Software Libraries," in Modern Software Tools in Scientific Computing, Edited by E. Arge, A.M. Bruaset and H.P. Langtangen, Birkhäuser Press, 1997, pp. 163–202.

Beam, R.M. and Warming, R.F., "An implicit finite-difference algorithm for hyperbolic systems in conservation-law form," J. Comput. Phys., Vol. 22, 1976, pp. 87-110.

Bhushan, S., Xing, T., Carrica, P., and Stern, F., "Model- and Full-scale URANS/DES Simulations for Athena R/V Resistance, Powering, and Motions," Proc. 9th International Conference on Numerical Ship Hydrodynamics, 2007, Ann Arbor, Michigan.

Carrica, P.M., Wilson, R.V., Noack, R., Xing, T., Kandasamy, M., Shao, J., Sakamoto, N., and Stern, F., "A Dynamic Overset, Single-Phase Level Set Approach for Viscous Ship Flows and Large Amplitude Motions and Maneuvering," Proc. 26th Symposium on Naval Hydrodynamics, 2006, Rome, Italy.

Carrica P.M., Wilson R.V. and Stern F., "An Unsteady Single-phase Level Set Method for Viscous Free Surface Flows," Int. J. Num. Meth. Fluids, Vol.53, 2007, pp.229-256.

Chang, Y.C., Hou, T.Y., Merriman, B., Osher S., "A Level Set Formulation of Eulerian Interface Capturing

Methods for Incompressible Fluid Flows," J. Comp. Phys., Vol. 124, 1996, pp. 449-464.
Choi, H. and Moin, P., "Effects of the Computational Time Step on Numerical Solutions of Turbulent Flow," J. Comput. Phys., Vol. 113, 1994, pp. 1-4.
D'Este, F. and Contento, G., "Time Domain Linear and Weakly Nonlinear Coupled Wave Resistance and Seakeeping Computations," Science and Supercomputing at CINECA, Report, 2003.
Dommermuth, D., T.T. O'Shea, D. Wyatt, M. Sussman, G. Weymouth, D. Yue, P. Adams, and R. Hand. "The Numerical Simulation of Ship Waves Using Cartesian-grid and Volume-of-fluid Methods," Proc. 26th Symposium on Naval Hydrodynamics, 2006, Rome, Italy.
Enright, D., Fedkiw, R., Ferziger, J., and Mitchell, I., "A Hybrid Particle Level Set Method for Improved Interface Capturing," J. Comput. Phys., Vol. 183, 2002, pp. 83-116.
Fu, T., Karion, A., Pence, A., Rice, J., Walker, D., and Ratcliffe, T., "Characterization of the Steady Wave Field of a High Speed Transom Stern Ship – Model 5365 Hull Form," naval Surface Warfare Center, Carderock Division, Hydromechanics Directorate R&D Report, NSWCCD-50-TR-2005, 2005.
Gui, L, Longo, J, and Stern, F., "Towing Tank PIV Measurement System, Data and Uncertainty Assessment for DTMB Model 5512," Exp. in Fluids, Vol.31, 2001, pp.336-346.
Haller, G. "An Objective Definition of a Vortex," J. Fluid Mech., Vol. 525, 2005, pp.1-26.
Huang, J., Carrica, P. M. and Stern, F. "Coupled Ghost Fluid/Two-Phase Level Set Method for Curvilinear Body Fitted Grids," Int. J. Num. Meth. Fluids, 2007, accepted, available online doi:10.1002/fld.1499.
Jiang, G.-S. and Peng, D., "Weighted ENO Schemes for HamiltonJacobi Equations," SIAM J. Sci. Comp., Vol. 21, 2000, pp. 2126-2143.
Jiang, G.-S. and Shu, C.-W., "Efficient Implementation of Weighted ENO Schemes," J. Comput. Phys., Vol. 126, 1996, pp. 202-228.
Kang, M., Fedkiw, R. and Liu, X. D., "A Boundary Condition Capturing Method for Multiphase Incompressible Flow," J. Sci. Comp., Vol. 15, 2000, pp. 323-360.
Kim, J., Kim, D., and Choi, H., "An Immersed-Boundary Finite-Volume Method for Simulations of Flow in Complex Geometries," J. Comput. Phys., Vol. 171, 2001, pp. 132-150.
Liu, X. D., Fedkiw, R., and Kang, M., "A Boundary Condition Capturing Method for Poisson's Equation on Irregular Domains," J. Comp. Phys., Vol. 160, 2000, pp. 151-178.
Longo, J., Shao, J., Irvine, M., and Stern, F., "Phase-Averaged PIV for the Nominal Wake of a Surface Ship in Regular Head Waves," J. Fluids Eng., Vol.129, 2007, pp.524-540.
MacNeice, P., Olson, K.M., Mobarry, C., deFainchtein, R., and Packer, C., "PARAMESH : A parallel adaptive mesh refinement community toolkit.", Computer Physics Communications, Vol. 126, 2000, pp. 330-354.
Mattor, N., Williams, T.J., and Hewett, D.W., "Algorithm for Solving Tridiagonal Matrix Problems in Parallel," Parallel Comput., Vol. 21, 1995, pp. 1769-1782.
Meneveau, C., Lund, C.S., and Cabot, W.H., "A Lagrangian Dynamic Subgrid-scale Model of Turbulence," J. Fluid Mech., Vol. 319, 1996, pp. 353-385.
Menter, F. R., "Two-Equation Eddy Viscosity Turbulence Models for Engineering Applications," AIAA J., Vol.32, 1994, pp.1598-1605.
Nikitin, N., "Finite-Difference Method for Incompressible Navier-Stokes Equations in Arbitrary Orthogonal Curvilinear Coordinates," J. Comp. Phys., Vol. 217, 2006, pp. 759-781.
Noack R., "SUGGAR: a General Capability for Moving Body Overset Grid Assembly," AIAA paper 5117, 2005.
Peng, D., Merriman, B., Osher, S., Zhao, H., and Kang, M., "A PDE-Based Fast Local Level Set Method," J. Comp. Phys., Vol. 155, 1999, pp. 410-438.
Peskin, C. S., "Flow Patterns Around Heart Valves: a Numerical Method," J. Comp. Phys., Vol. 10, 1972, pp. 252-271.
Shu, C. W. and Osher, S., "Efficient Implementation of Essentially Non-oscillatory Shock-capturing Schemes," J. Comp. Phys., Vol. 77, 1988, pp. 439-471.
Sussman, M., "A parallelized, adaptive algorithm for multiphase flows in general geometries," Computers & Structures, Vol. 83, 2005, pp. 435-444.
Sussman, M., Smereka, P. and Osher, S., "A Level Set Approach for Computing Solutions to Incompressible Two-Phase Flow," J. Comp. Phys., Vol. 114, 1994, pp. 146-159.
Swarztrauber, P., "Fast Fourier Transforms Algorithms for Vector Computers," Parallel Computing, Vol. 1, 1984, pp.45-63.
Swarztrauber, P. and Sweet, R., "Efficient FORTRAN Subprograms for the Solution of Elliptic Partial Differential Equations", NCAR Technical Note-TN/IA-109, July 1975
Wilson, W., Fu, T.C., Fullerton, A., and Gorski, J., "The Measured and Predicted Wave Field of Model 5365: An Evaluation of Current CFD Capability," Proc. 26th Symposium on Naval Hydrodynamics, 2006, Rome, Italy.
Wilson, R.V., Carrica, P.M. and Stern, F., "URANS Simulations for a High-Speed Transom-Stern Ship with Breaking Waves," Int. J. of Comp. Fluid Dyn., Vol. 20, No. 2, 2006, pp.105-125.

Xing, T., Shao, J., and Stern, F., "Reynolds Stress/DES Simulation of Unsteady Vortical Flow around Obliquely Towed Kriso Tanker Hull KVLCC2," Proc. 9th International Conference on Numerical Ship Hydrodynamics, 2007, Ann Arbor, Michigan.

Yang, J. and Balaras, E., "An Embedded-Boundary Formulation for Large-eddy Simulation of Turbulent Flows Interacting with Moving Boundaries," J. Comp. Phys., Vol. 215, 2006, pp. 12-40.

Yang, J., and Stern, F., "Large-Eddy Simulation of Breaking Waves Using Embedded-Boundary/Level-Set Method," Proc. 45th AIAA Aerospace Sciences Meeting and Exhibit, paper 2007-1455, 2007, Reno, Nevada.

Yang, J., and Stern, F., "A Sharp Interface Method for Two-Phase Flows Interacting with Moving Bodies," Proc. 18th AIAA Computational Fluid Dynamics Conference, paper 2007-4578, 2007, Miami, Florida.

Table 1 Test matrix

Test	Model	*Fr*	Grid	Code type
1	Wigley	0.267	F	Cartesian, NS
2			C	Cartesian, NS
3			C+B	Body-fitted, RANS
4	5365	0.25	F	Cartesian, NS
5	5512	0.28	M	Semi-coupled, LES

Table 2 Grid details

Grid name	Grid type	*i*	*j*	*k*
F	Cartesian, fine grid	512	120	120
M	Cartesian, medium grid	256	104	104
C	Cartesian, coarse grid	256	68	68
B	Body-fitted grid	161	79	75

Table 3 Domain sizes

Test	Axial	Spanwise	Vertical
1,4	$-1\le z\le 2.5$	$0\le y\le 1.3$	$-0.845\le x\le 0.045$
2,3	$-0.8\le z\le 2.5$	$0\le y\le 1.3$	$-0.8\le x\le 0.04$
5	$-1\le z\le 2.5$	$-0.72\le y\le 0.72$	$-0.72\le x\le 0.72$

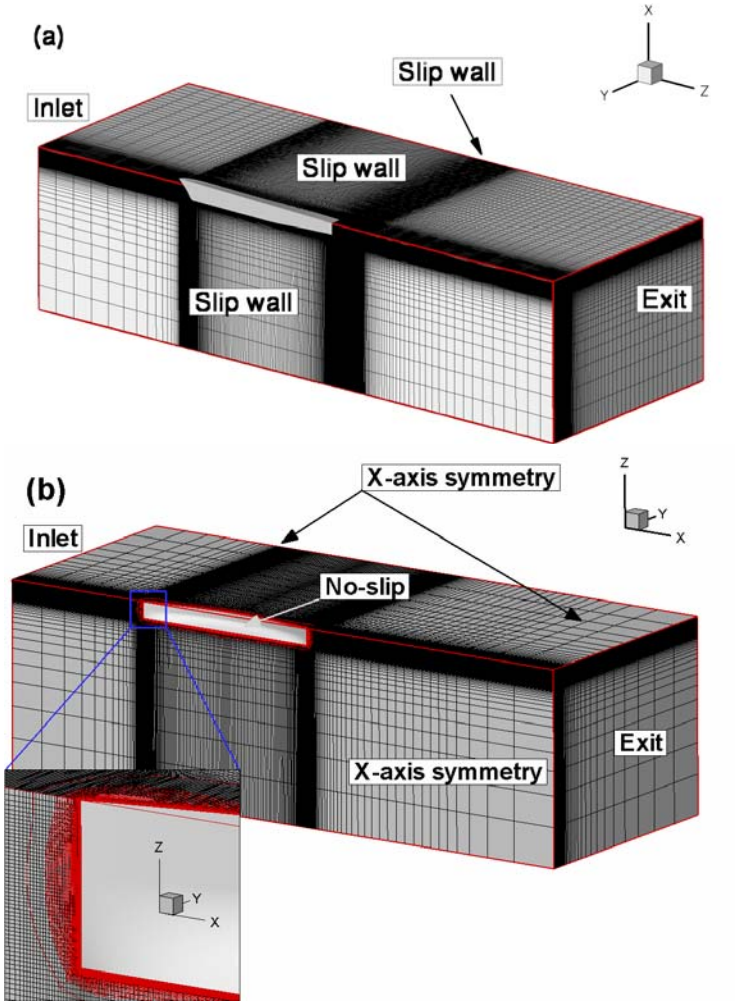

Figure 1: Grid topology and boundary conditions:
(a) Cartesian fine grid, (b) body-fitted grid with Cartesian coarse grid.

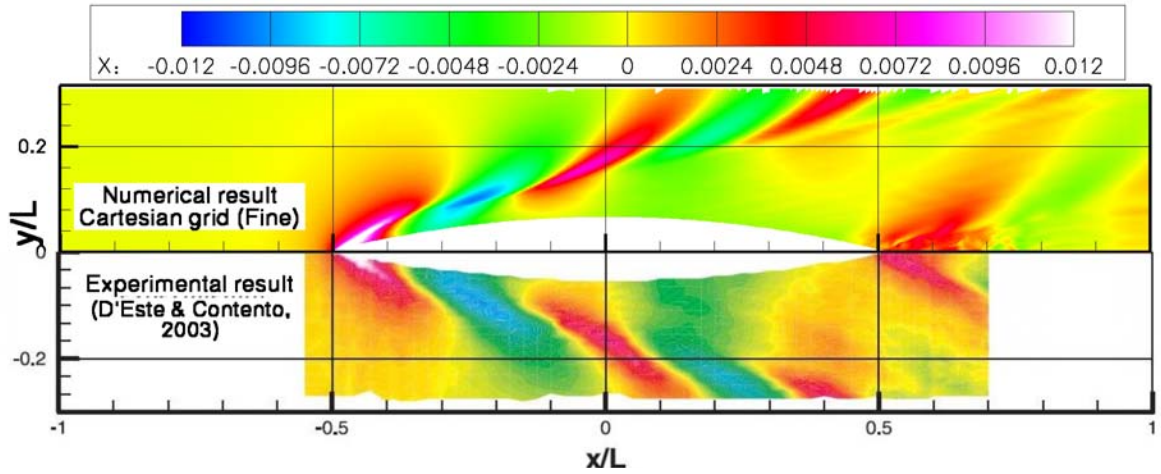

Figure 2: Wave field comparison of Cartesian fine grid NS solution (top) and experimental data (bottom).

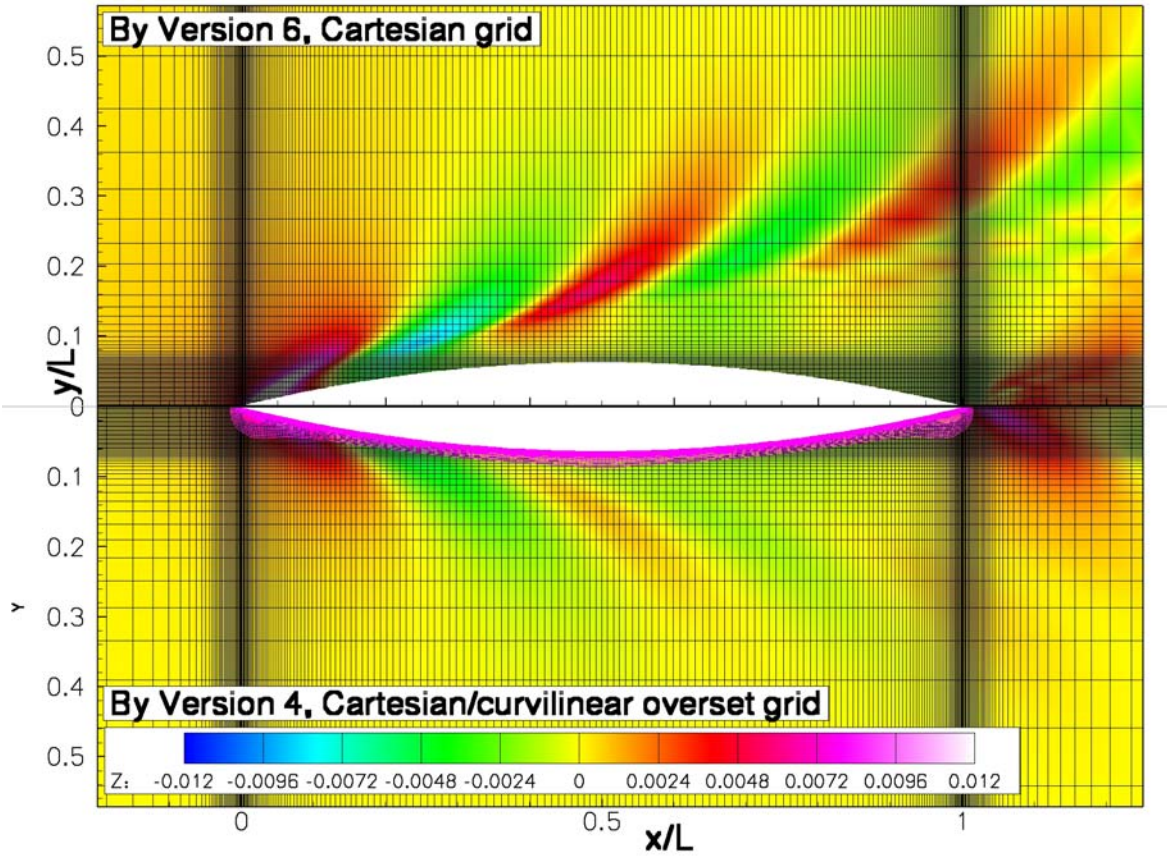

Figure 3: Wave field comparison of Cartesian coarse grid NS solution (top) and body-fitted grid RANS solution (bottom).

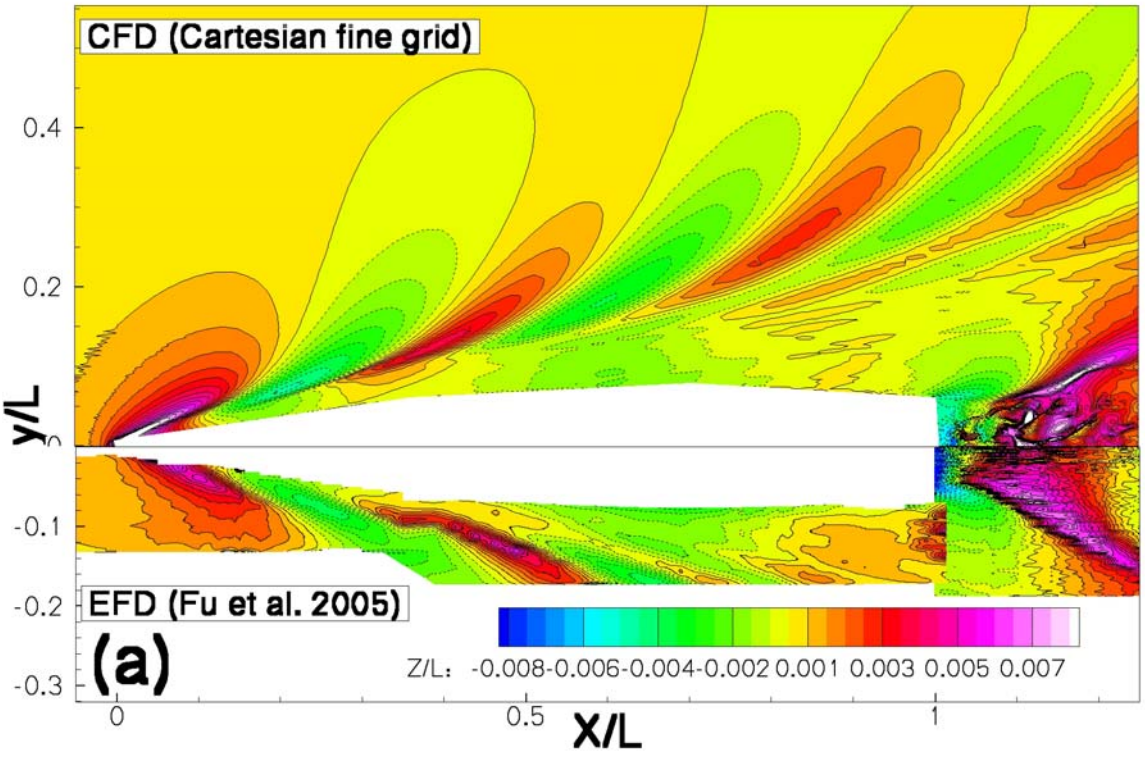
CFD (Cartesian fine grid)
EFD (Fu et al. 2005)
(a)
Z/L: -0.008-0.006-0.004-0.002 0.001 0.003 0.005 0.007
y/L
X/L
0.4
0.2
0
-0.1
-0.2
-0.3
0
0.5
1

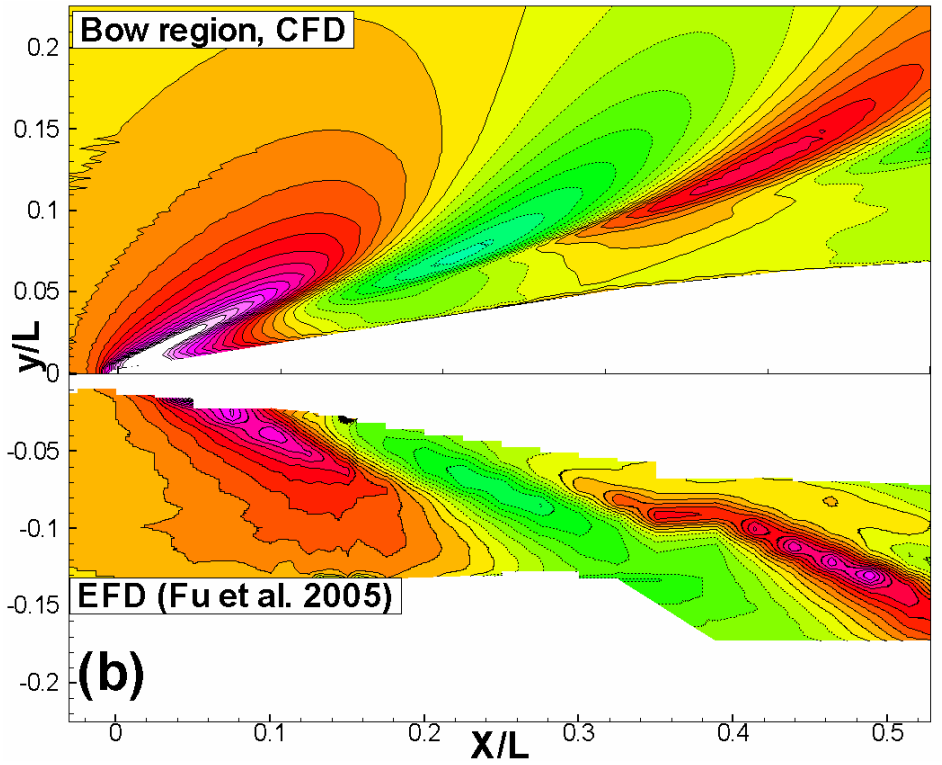
Bow region, CFD
EFD (Fu et al. 2005)
(b)
y/L
X/L
0.2
0.15
0.1
0.05
0
-0.05
-0.1
-0.15
-0.2
0
0.1
0.2
0.3
0.4
0.5

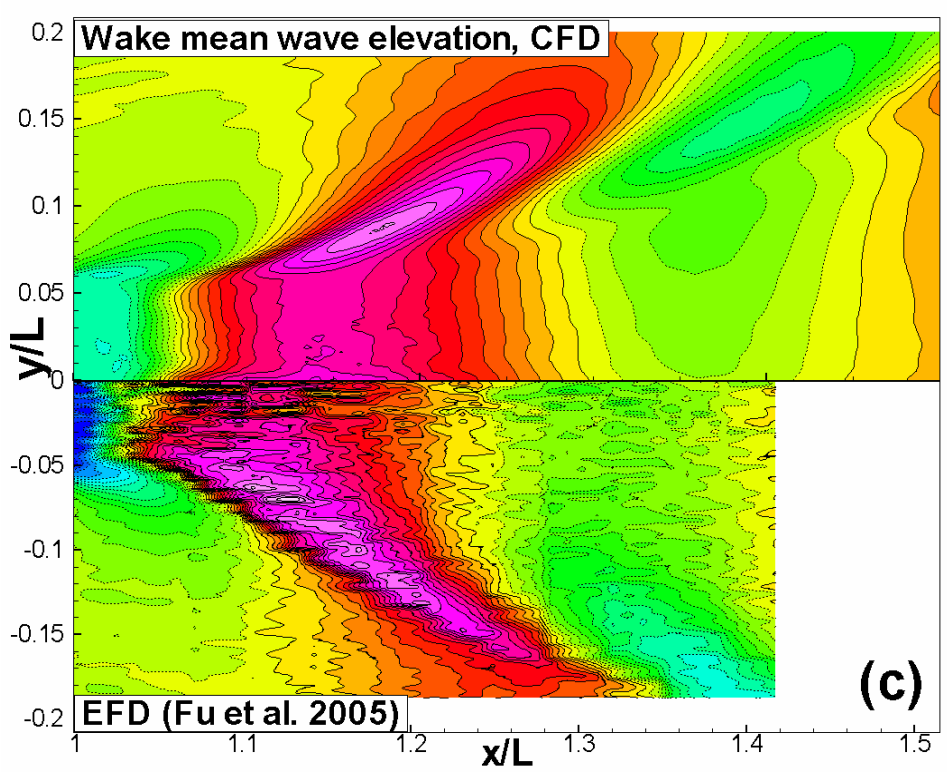

Figure 4: Wave field comparison of Cartesian fine grid NS solution and experimental data: (a) instantaneous whole domain, (b) instantaneous bow region, (c) mean wake region.

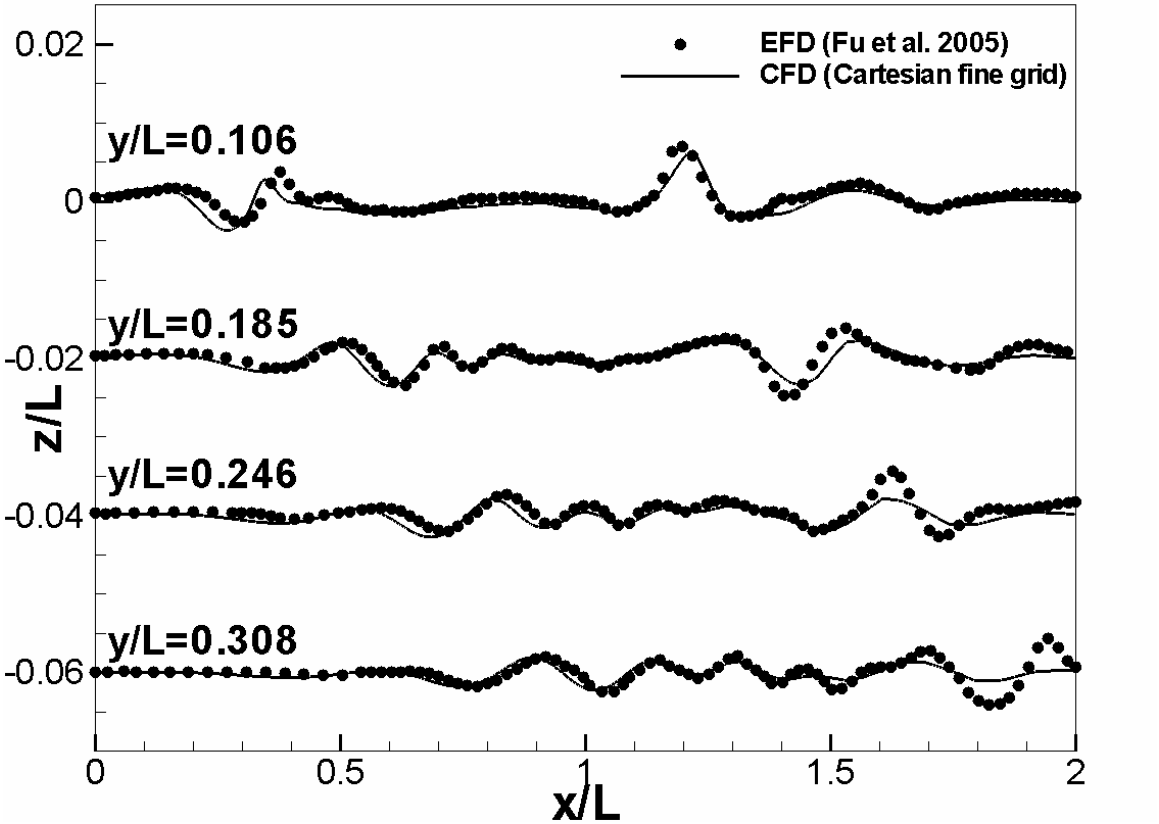

Figure 5: Wave cuts at different cross planes.

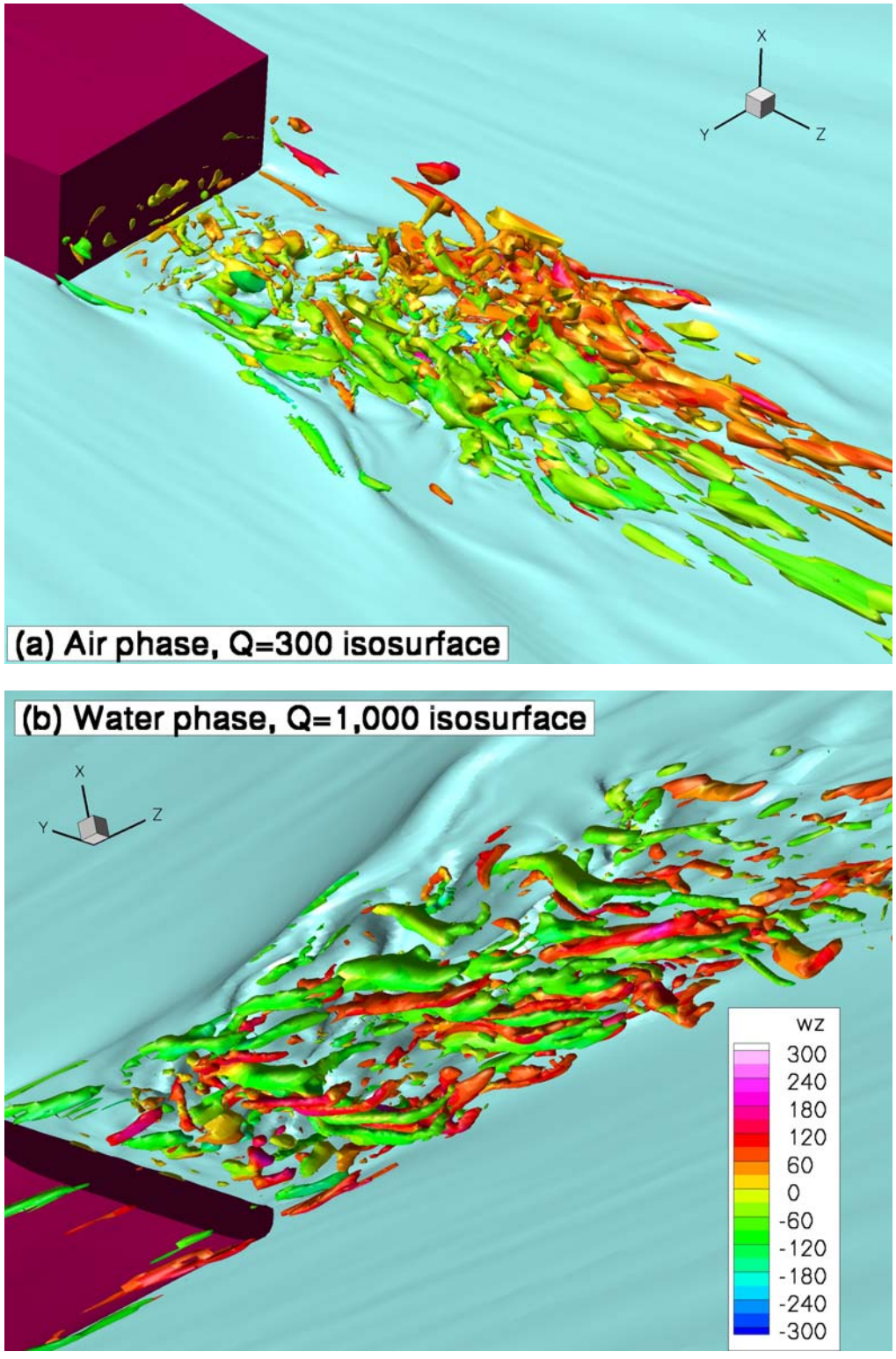

Figure 6: Instantaneous vortical structures in air (a) and water (b).

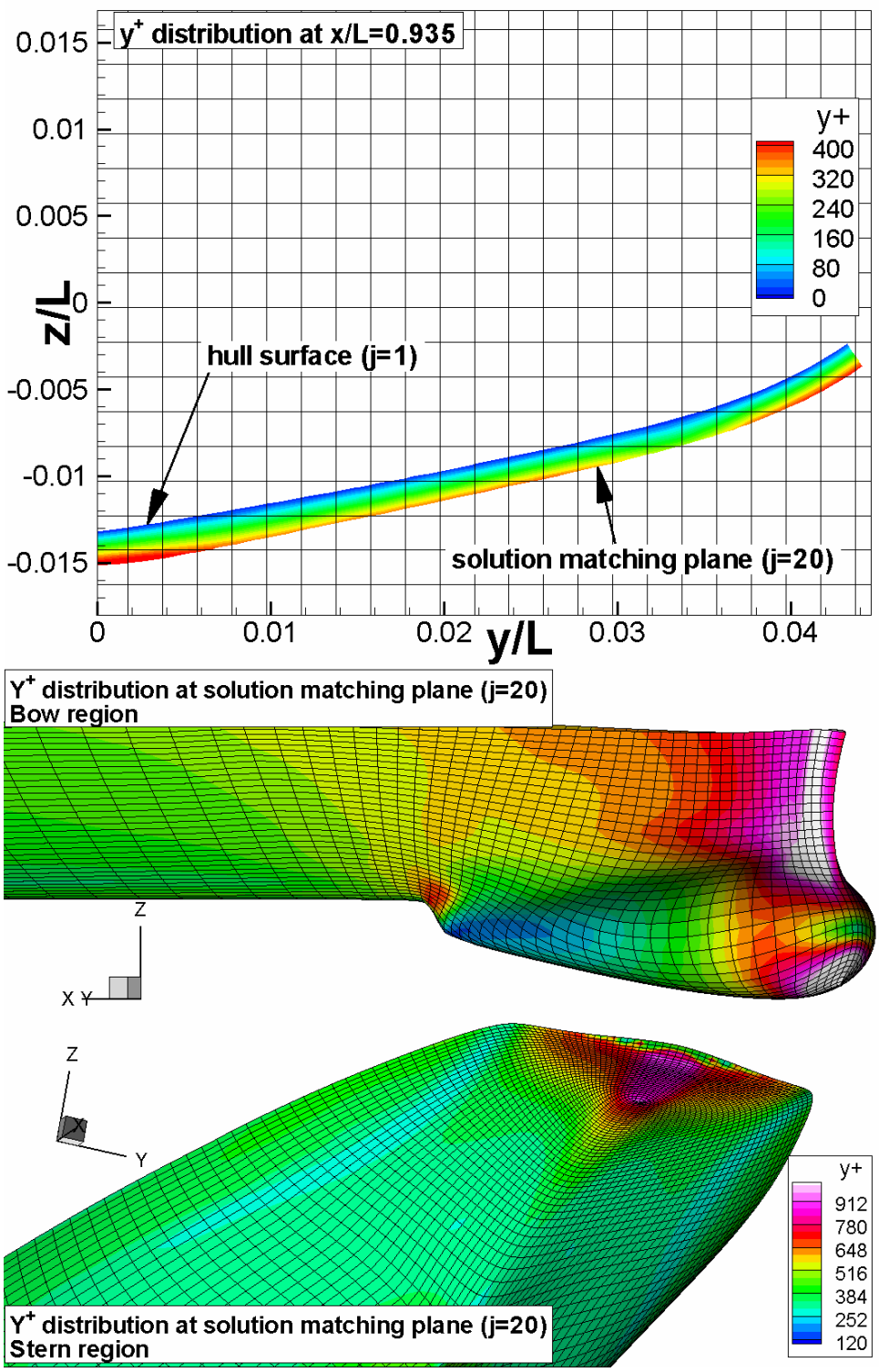

Figure 7: y+ distribution at the solution matching surface between body-fitted grid and Cartesian grid: 2D perspective at x/L=0.935 (top) and 3D perspective of bow and stern regions (bottom).

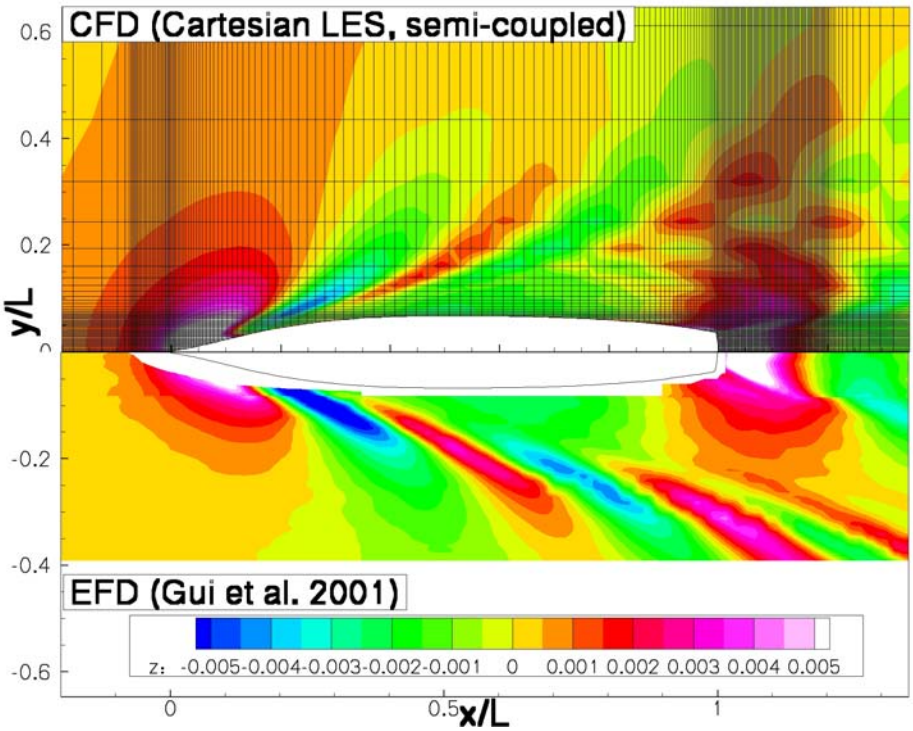

Figure 8: Wave field comparison of Cartesian LES solution (top) and experimental data (bottom).

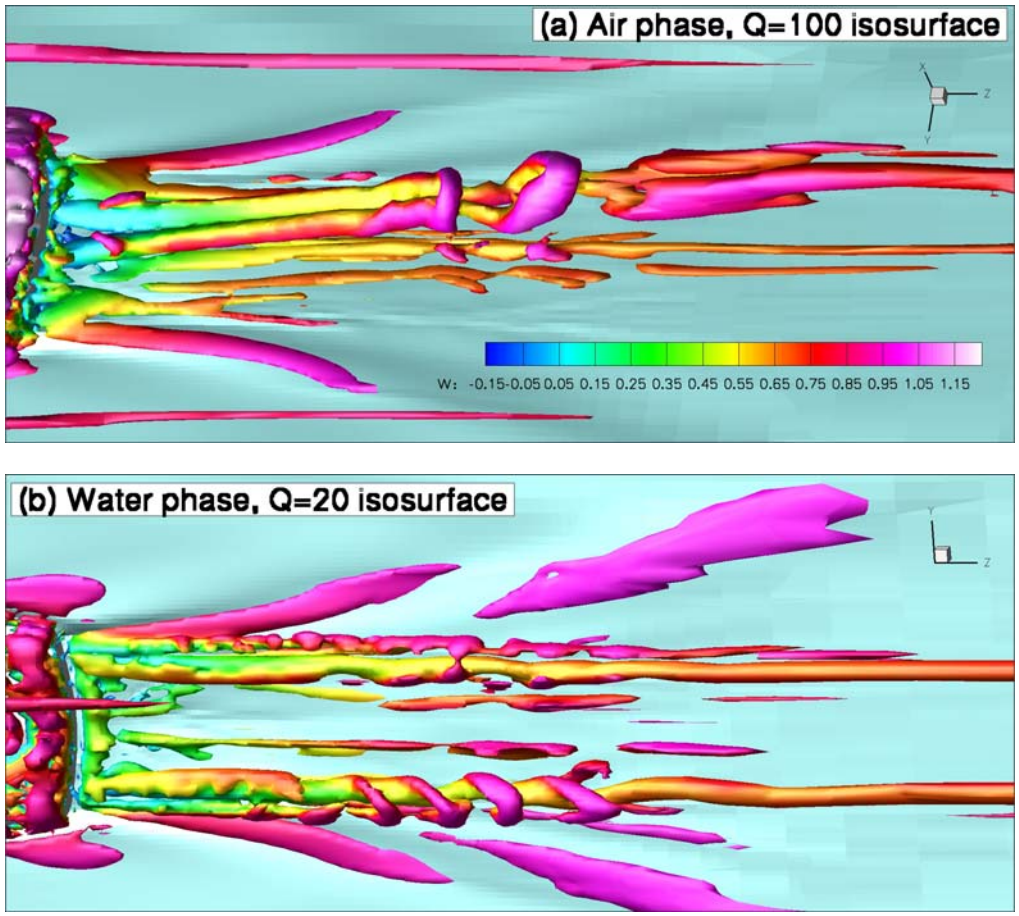

Figure 9: Instantaneous vortical structures in air (a) and water (b).

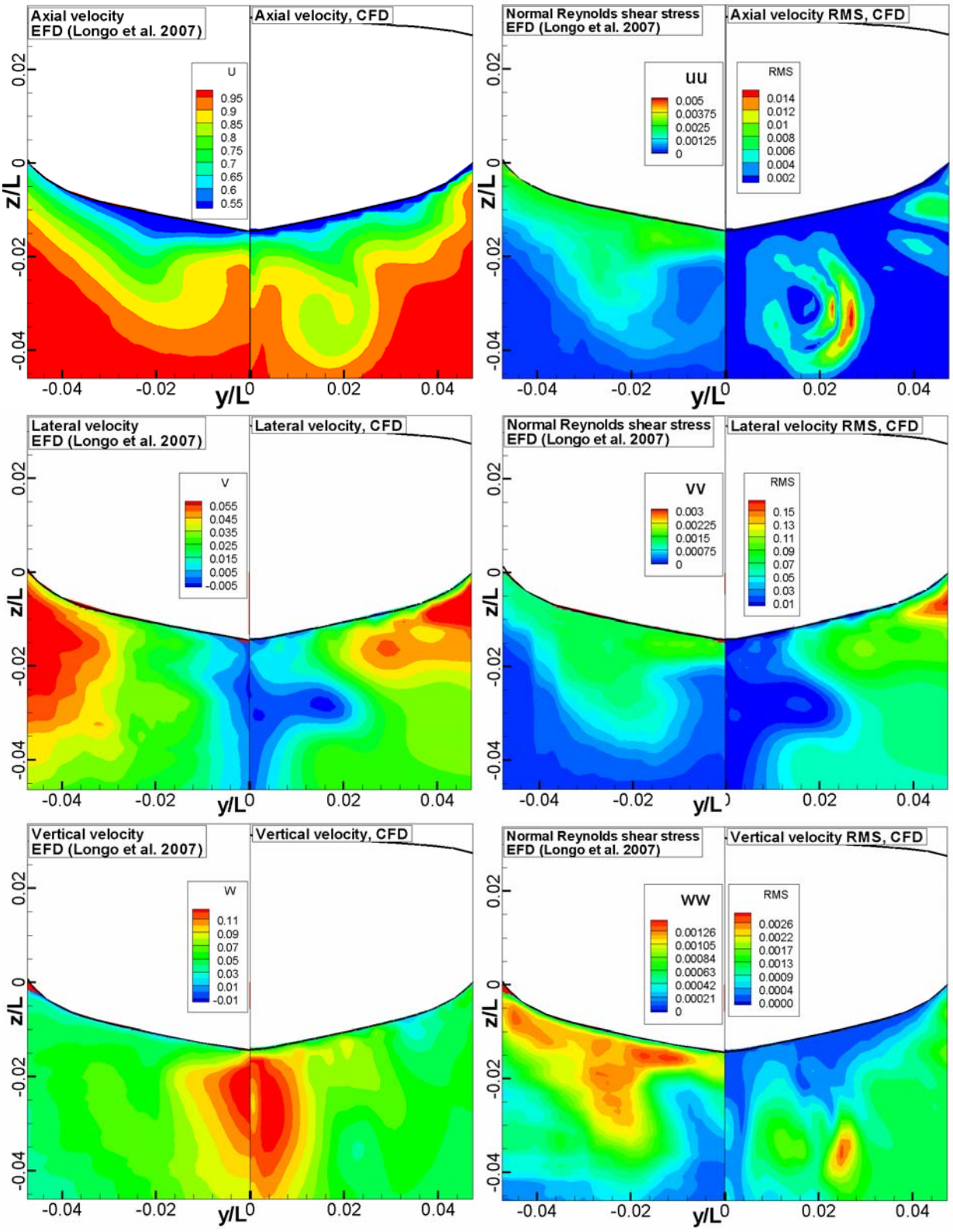

Figure 10: Average velocity profiles (left) and RMS fluctuations (right)
from Cartesian LES solution and experiments.